THE JOURNAL OF PHYSICAL CHEMISTRY B

pubs.acs.org/JPCB

Article

Assessing the Location of Ionic and Molecular Solutes in a Molecularly Heterogeneous and Nonionic Deep Eutectic Solvent

Published as part of The Journal of Physical Chemistry virtual special issue "Deep Eutectic Solvents".

Xiaobing Chen,[†] Yaowen Cui,[†] Habtom B. Gobeze, and Daniel G. Kuroda*

Cite This: *J. Phys. Chem. B* 2020, 124, 4762–4773

Read Online

ACCESS | Metrics & More | Article Recommendations | Supporting Information

ABSTRACT: Deep eutectic solvents (DES) are emerging sustainable designer solvents viewed as greener and better alternatives to ionic liquids. Nonionic DESs possess unique properties such as viscosity and hydrophobicity that make them desirable in microextraction applications such as oil-spill remediation. This work builds upon a nonionic DES, NMA–LA DES, previously designed by our group. The NMA–LA DES presents a rich nanoscopic morphology that could be used to allocate solutes of different polarities. In this work, the possibility of solvating different solutes within the nanoscopically heterogeneous molecular structure of the NMA–LA DES is investigated using ionic and molecular solutes. In particular, the localized vibrational transitions in these solutes are used as reporters of the DES molecular structure via vibrational spectroscopy. The FTIR and 2DIR data suggest that the ionic solute is confined in a polar and continuous domain formed by NMA, clearly sensing the direct effect of the change in NMA concentration. In the case of the molecular nonionic and polar solute, the data indicates that the solute resides in the interface between the polar and nonpolar domains. Finally, the results for the nonpolar and nonionic solute ($W(CO)_6$) are unexpected and less conclusive. Contrary to its polarity, the data suggest that the $W(CO)_6$ resides within the NMA polar domain of the DES, probably by inducing a domain restructuring in the solvent. However, the data are not conclusive enough to discard the possibility that the restructuring comprises not only the polar domain but also the interface. Overall, our results demonstrate that the NMA–LA DES has nanoscopic domains with affinity to particular molecular properties, such as polarity. Thus, the presented results have a direct implication to separation science.

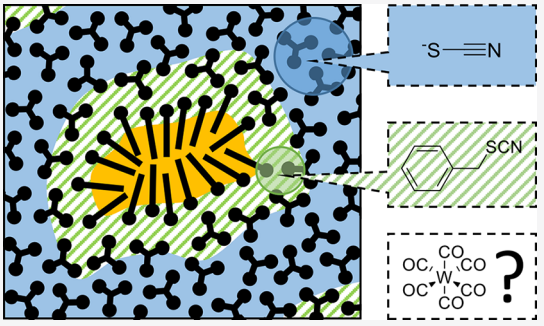

INTRODUCTION

Deep eutectic solvents (DESs) are a new class of sustainable designer solvents with characteristics and physical properties similar to those of ionic liquids (IL), but DESs are inherently different in their formation mechanism, composition, and applications. Unlike ILs, which are entirely formed by a fixed and discrete ratio between the anion and cation, DESs are eutectic mixtures composed of ionic and/or nonionic species.[1] It is now accepted that the hydrogen bond interaction between the different DES components reduces the enthalpic component of the energetics, which results in the depression of the melting point of the mixture and gives a DES its liquid state at ambient temperature.[1−3] Thus, DESs are simple and low-cost alternatives to ILs because they can be readily made by mixing two components. This last characteristic makes them more appealing than ILs because the latter usually require complex synthetic procedures for their preparation. Moreover, DESs have an added flexibility, since one can select specific components with a range of desirable properties such as low cost, renewability, biodegradability, and low toxicity. As such, DESs can be designed according to a tailored application.[4−6] Hence, DESs have received a remarkable interest since they were first introduced by Abbott and coworkers in 2002.[7] DESs have been extensively studied for their applications in green chemistry,[6,8−11] organic synthesis,[12−17] material preparation,[18−23] electrochemistry,[24−27] and analytical and separation sciences.[28−34]

Archetypal DESs, based on mixtures of quaternary ammonium or metal salt and a hydrogen bond donor or metal chloride, have been intensely studied in the past decade.[7,35] These DESs are commonly known as "ionic" DESs. Recently, hydrophobic DESs have started to receive immense attention because of their unique properties (e.g., hydrophobicity, viscosity, and density) and their promising applications in microextraction techniques.[6,36,37] Hydrophobic DESs made from a fatty acid and several quaternary

Received: March 20, 2020
Revised: May 13, 2020
Published: May 18, 2020

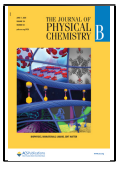

https://dx.doi.org/10.1021/acs.jpcb.0c02482
J. Phys. Chem. B 2020, 124, 4762–4773

ammonium salts have shown to be suitable as a water-immiscible extraction medium for volatile fatty acids, such as propionic and butyric acids, in diluted aqueous solutions.[36] The high hydrophobicity of these DESs, manifested by their low water content on mixing with water (~1.8 wt %) and their low leaching of quaternary ammonium salt (~1.9 wt %), has proven to be vital in defining their extraction efficiency, as the efficiency increases with increasing hydrophobicity. Furthermore, the low leaching of the ionic component has provided further evidence of the strong interactions between the ionic and molecular components of the DES, in agreement with the proposed interactions occurring in archetypal choline chloride based DES. Interestingly, other hydrophobic DESs without ionic components have also shown notable extraction properties.[38]

Recently, a newly designed nonionic DES formed by the simple combination of an amide (*N*-methylacetamide) and a long-chain carboxylic acid (lauric acid) was demonstrated.[39] This DES made from inexpensive, biodegradable, and low-toxicity feed stock materials has proven an efficient gelator for selectively phasing out the oil phase in an oil−water mixture. Moreover, this DES has a promising potential application in oil-spill remediation, since its performance is on a par with that of currently used or state-of-the-art gelators.[39] The molecular structure, dynamics, and interactions of this NMA−LA DES have been investigated in depth using linear and time-resolved IR spectroscopies along with small-angle X-ray scattering techniques.[40] The NMA−LA DES, which has a minimum fusion point of ~6 °C at an LA/NMA molar ratio of approximately 1:4, has been found to have a hydrogen-bond network between the two molecular components, NMA and LA, even though the interaction between NMA and LA in this nonionic DES was found to be weak, favored only by ~1 kJ/mol with respect to the pure components.[40] The structure and dynamics study of the NMA−LA DES revealed interesting nanoscopic details about the morphology of the mixture. In particular, it has been observed that the NMA−LA DES has molecular heterogeneities due to the presence of polar and nonpolar domains formed by NMA and LA, respectively, which interact via hydrogen bonds at the interface. The structure observed for the NMA−LA DES departs from that of another nonionic DES composed of acetamide and urea, which showed structural and dynamical homogeneity.[41] However, in the case of the acetamide−urea DES, the structural similarity between the two components provides a reasonable framework to explain why the components mix evenly and form a homogeneous molecular environment.

The interesting heterogeneous structure of the NMA−LA DES provides a molecular landscape with different features that could accommodate different solutes with preferential affinity to the particular domains (nonpolar or polar) in the mixture. This work is aimed at characterizing the location of different solutes within the nanoheterogeneous NMA−LA DES structure using IR spectroscopy. To this end, three solutes with different polarities and natures of intermolecular interactions are used in combination with DESs having different ratios of LA/NMA, which correspond to solutions with concentrations of LA below and at the eutectic point.[40] The selected solutes (Scheme 1) are tetrabutylammonium thiocyanate (TBASCN), benzyl thiocyanate (BSCN), and tungsten hexacarbonyl ($W(CO)_6$). The selection of these solutes is based on each having vibrational modes with sensitivity to structural and dynamical changes in the molecular environment.[42−53] In particular, the thiocyanate ion (SCN^-) has been extensively used as an infrared probe in a variety of different systems, such as molecular solvents and ionic liquids.[42−47,54] Moreover, it has been previously demonstrated that the tetrabutylammonium cation (TBA^+) causes negligible perturbation to the solvation of the thiocyanate ion.[42] In the case of BSCN, generally organic thiocyanates are shown to be good infrared probes to study solvent dynamics and site-specific changes at interfaces.[55,56] Finally, $W(CO)_6$ has been successfully utilized to probe the structure of nonpolar domains, such as those found in bilayers.[49−53] The IR active mode of CO stretch was previously shown to be a triply degenerate (T_{1u}), vibrationally coupled, and delocalized mode, which is referred to as CO asymmetric stretch in this work.[57,58] In addition, the nearby Raman active mode of CO stretch is a doubly degenerate mode with E_g symmetry, which is referred to as CO symmetric stretch here.[57,59] Moreover, the vibrational dynamics, energy relaxation, and intra-/intermolecular energy transfer of the CO asymmetric stretch mode of $W(CO)_6$ was previously characterized via ultrafast IR spectroscopy.[57]

Scheme 1. Structures of Solvents and Solutes[a]

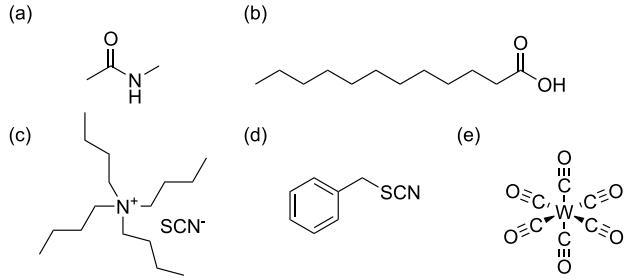

[a](a) NMA, (b) LA, (c) TBASCN, (d) BSCN, and (e) $W(CO)_6$.

In previously reported works, the molecular environment around a solute in a DES has commonly been derived from time-resolved fluorescence emission spectroscopy, where the solutes act as probes by reporting changes in fluorescence lifetime and anisotropy dynamics depending on the nature of their local environment.[60−63] Here, Fourier-transform infrared spectroscopy (FTIR) and vibrational echo two-dimensional infrared (2DIR) spectroscopy are used to study the vibrational dynamics of the three solutes. Furthermore, the 2DIR spectra provide information about the dynamical processes observed by the solutes (probes), including solvent dynamics and chemical exchange, which are important not only to describing the molecular interactions and motions in sub- or picosecond time scale but also to assessing where the solutes reside.[64,65]

METHODS

Sample Preparation. LA (Alfa Aesar, 99.5%) and NMA (Alfa Aesar, 99%) were used as received. The two components were mixed at varied ratios as listed in Table 1, in which DES2 and DES4 correspond to the concentrations of LA below and

Table 1. Compositions and Abbreviations of the Investigated Solvents

sample	molar ratio of NMA/LA
DES2	2:1
DES4	4:1
NMA	1:0

https://dx.doi.org/10.1021/acs.jpcb.0c02482
J. Phys. Chem. B 2020, 124, 4762−4773

at the eutectic point. The DESs were prepared by mixing two components in a vial with vortex mixer and sonicator. The solutes, TBASCN (TCI, 95%), BSCN (TCI, 99%), and $W(CO)_6$ (Pressure Chemical Co, 98%), were used without further purification. The concentration of the two thiocyanate solutes was ∼100 mM. Due to the overall low solubility of $W(CO)_6$, the samples of $W(CO)_6$ were prepared by adding the metal carbonyl to the DES, followed by a filtration with 0.2 μm PTFE membrane filter. All the DESs and chemicals were stored and prepared in a nitrogen-flushed glovebox.

Linear IR Spectroscopy. Linear IR measurements were performed using a Bruker Tensor 27 with a liquid-nitrogen-cooled narrow-band MCT detector. All samples were measured with 0.5 cm^{-1} resolution and averaged from 40 scans. The DES samples were measured at room temperature, while the NMA samples were measured at ∼30 °C using a temperature-controlled sample cell (Harrick Scientific). All samples were held in an O-ring-sealed sample cell with two CaF_2 windows separated by different-thickness Teflon spacers. All sample cells were prepared in a nitrogen-filled glovebox to minimize exposure to moisture.

2DIR Spectroscopy. The setup used for 2DIR experiments has been previously detailed in the literature, so only a short description is provided here.[66] The input IR pulses were generated with a Spectra Physics Spitfire Ace Ti:sapphire amplifier at a repetition rate of 5 kHz, in combination with an OPA-800C and difference-frequency-generation crystal. The input IR beam was split into three replicas, which were later focused on the sample using the well-known boxcars geometry.[67] The photon echo signal was measured in the $-\mathbf{k}_1 + \mathbf{k}_2 + \mathbf{k}_3$ phase-matching direction. A heterodyned detection was performed using a fourth pulse (local oscillator). The heterodyned signal was measured in a 64-element MCT array detector after dispersing the heterodyned signal in a spectrometer. The photon echo signal was measured as a function of three critical time intervals: the coherence time τ (interval between pulses 1 and 2), the waiting time T_w (interval between pulses 2 and 3), and the coherence time t (interval between pulse 3 and the detected signal). These time intervals were set via computer-controlled translation stages. Here, 2DIR data were collected by scanning τ time from −4 to +4 ps for TBASCN and BSCN samples and from −3 to +3 ps for $W(CO)_6$ samples in increments of 5 fs for each waiting time to collect both the rephasing and nonrephasing data by switching the time ordering.[66] Signals were collected for waiting times from 0 to 100 ps with exponential time steps. In all measurements, the local oscillator always preceded the photon echo signal by ∼0.6 ps. The time domain signal, collected as a function of (τ, T, λ_t) via a monochromator-array detection, is transformed into the 2DIR spectra $(\omega_\tau, T, \omega_t)$ by means of Fourier transforms. A detailed explanation of the Fourier analysis has been described elsewhere.[68] All sample cells used in the 2DIR experiments were prepared using the methodology as previously described.

DFT Calculation. DFT calculations were performed with Gaussian 16 software at the B3LYP level of theory.[69] The 6-311+G(2d) basis set was used on carbon, oxygen, nitrogen, and hydrogen atoms, while the LANL2DZ basis set was utilized on tungsten atom.[70] Initial molecules and solvation shells were built in Avogadro software, where the structures were first minimized using a classical force field (MMFF94). Geometry optimizations and frequency calculations were performed in the gas phase.

RESULTS

The IR vibrational transition of the different solutes in DESs with different NMA/LA molar ratios were first investigated via linear IR spectroscopy (Figure 1). In this case, the nitrile

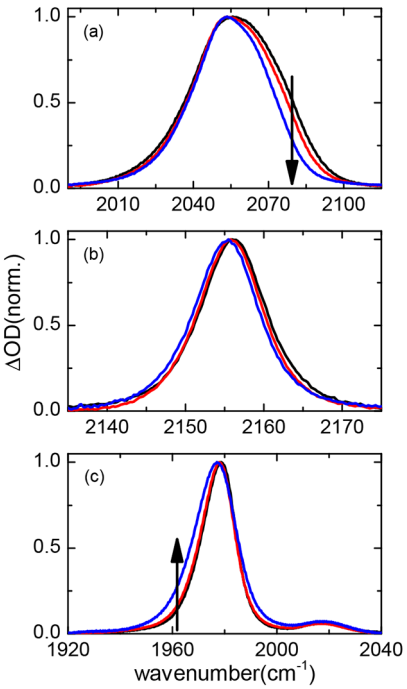

Figure 1. FTIR spectra after background subtraction and normalization of the different solutes in DESs. From top to bottom: spectra of TBASCN (a), BSCN (b), and $W(CO)_6$ (c) in DES2 (black), DES4 (red), and NMA (blue), respectively.

stretches of TBASCN and BSCN and the carbonyl asymmetric stretch of $W(CO)_6$ were used as infrared reporters. For comparison, the FTIR spectra of the solutes in neat NMA were also reported.

The FTIR spectra of the ionic solute (TBASCN) reveals an asymmetric line shape for the CN stretch with a shoulder on the blue-side of the spectra (Figure 1a). The CN stretch of the thiocyanate ion is substantially broad as revealed in its full width at half-maximum (fwhm), which ranges from ∼36 cm^{-1} in neat NMA to ∼43 cm^{-1} in DES2. The fwhm demonstrates that the CN stretch band becomes narrower with increasing NMA concentration in the solution. The broadening of the CN stretch band is accompanied by a change in the frequency of the maximum as seen in DES2 where the maximum is located at 2056 cm^{-1}, but in DES4 and neat NMA, the maxima are positioned at 2053 cm^{-1}. In addition, the second derivative of the spectra reveals the presence of two underlying peaks in this region (see the Supporting Information).

The polar and nonionic solute (BSCN) in the different solutions has an IR spectra with a symmetric band in the CN stretch region that slightly varies its frequency maxima and fwhm with increasing concentration of NMA (see Figure 1b and the Supporting Information). Overall, the CN stretch band of BSCN slightly shifts to a lower frequency and becomes slightly narrower when the concentration of NMA is increased in the solution, but the difference in the characteristics of this band for DES2 and DES4 is minor (see the Supporting Information).

https://dx.doi.org/10.1021/acs.jpcb.0c02482
J. Phys. Chem. B 2020, 124, 4762−4773

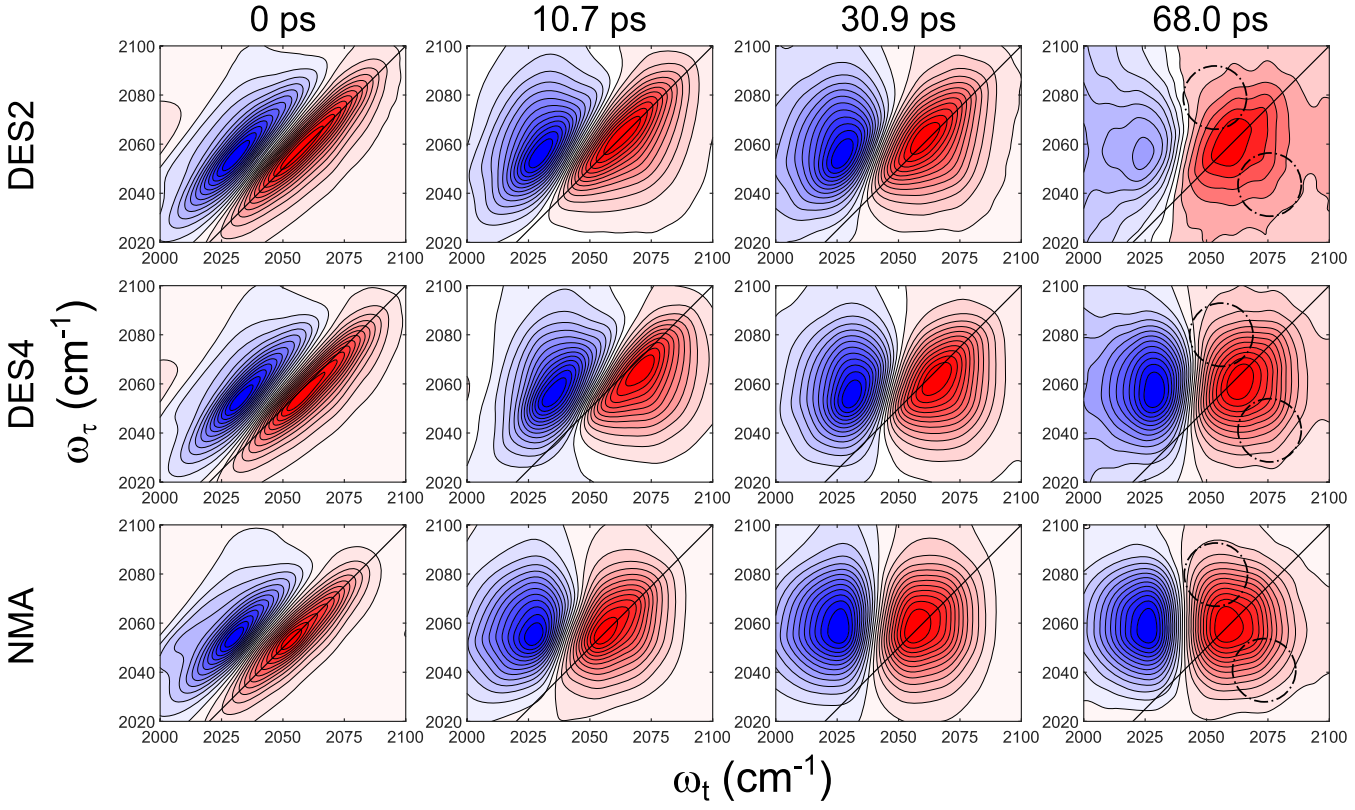

Figure 2. 2DIR spectra of TBASCN in DES2 (top), DES4 (middle), and NMA (bottom) at T_w = 0, 10.7, 30.9, and 68 ps. *y*-axis: pump frequency or ω_τ. *x*-axis: probe frequency or ω_t. The cross peaks are circled in the spectra at 68 ps.

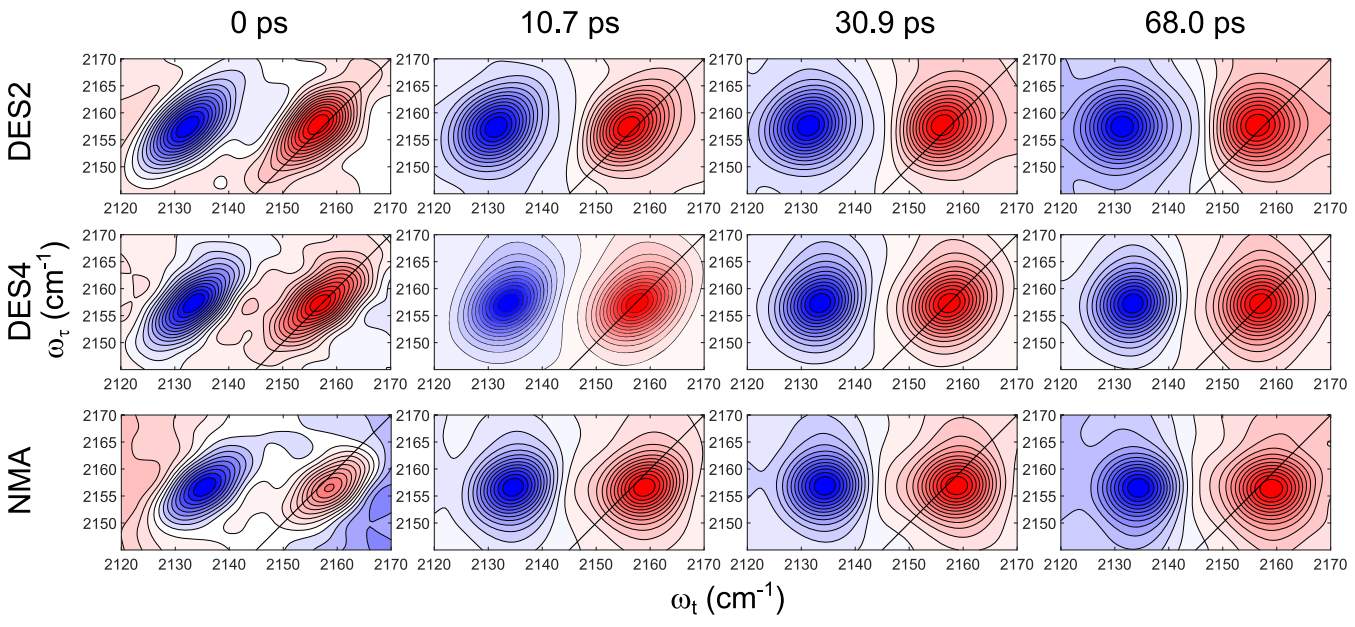

Figure 3. 2DIR spectra of BSCN in DES2 (top), DES4 (middle), and NMA (bottom) at T_w = 0, 10.7, 30.9, and 68 ps. *y*-axis: pump frequency or ω_τ. *x*-axis: probe frequency or ω_t.

The FTIR spectra of the nonionic solute ($W(CO)_6$) in the region of the CO asymmetric stretch (Figure 1c) reveal two bands with a main band located at ~1980 cm^{-1} and a side band at ~2020 cm^{-1}. The main band, which has been previously assigned to the CO asymmetric stretch,[49−53] has a slight asymmetric line shape in all studied solvents, with its features being almost identical to those in DES2 and DES4 but slightly different in NMA as seen in its fwhm (see the Supporting Information). The CO asymmetric stretch is broader in NMA compared to those in DES2 and DES4, which is opposite to the trend presented by the other two solutes. While the presence of the asymmetric CO is expected, the weak side peak at high frequency is not because $W(CO)_6$ has only three IR-allowed degenerate asymmetric CO stretches.[59,71,72] Interestingly, the high-frequency peak shows

https://dx.doi.org/10.1021/acs.jpcb.0c02482
J. Phys. Chem. B 2020, 124, 4762−4773

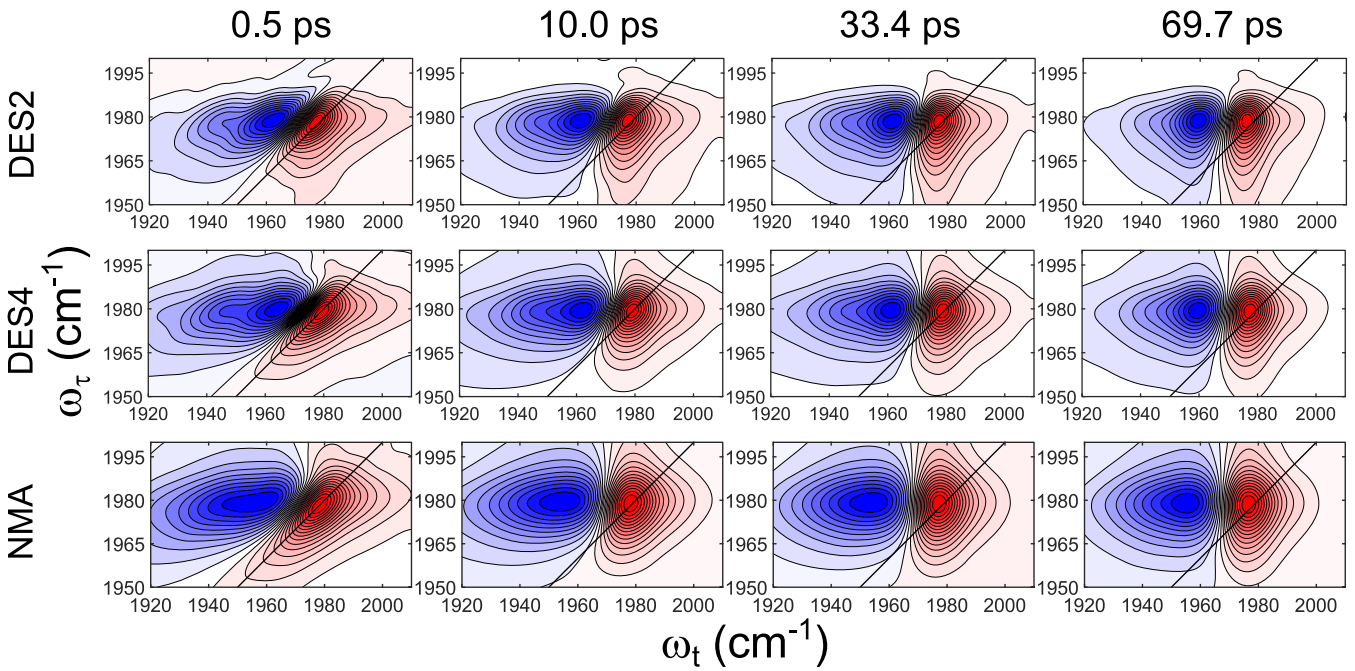

Figure 4. 2DIR spectra of $W(CO)_6$ in DES2 (top), DES4 (middle), and NMA (bottom) at T_w = 0.5, 10.0, 33.4, and 69.7 ps. *y*-axis: pump frequency or ω_τ. *x*-axis: probe frequency or ω_t.

a small increase in its amplitude when the solvent is switched from DESs to NMA.

More detailed insights into the structure and dynamics of the ionic and nonionic solutes in different solvents are gained via 2DIR spectroscopy. Figure 2 shows the 2DIR spectra of TBASCN in the CN stretching region for the three solutions. In the 2DIR spectra, the peaks close to the diagonal ($\omega_t = \omega_\tau$, black line in Figure 2) and depicted as red (positive) are due to vibrational transitions from $\nu = 0$ to $\nu = 1$, while the blue peaks (negative) shifted to lower frequencies are due to the anharmonically shifted $\nu = 1$ to $\nu = 2$ transitions.[64] Overall, the spectra of TBASCN in the three solutions reveal a main peak along the diagonal which is substantially broadened when the NMA concentration is increased, which is in direct agreement with the trend observed in FTIR (Figure 1). The spectra acquired at four different waiting times (T_w of 0, 10.7, 30.9, and 68.0 ps) show that the positive and negative peaks are initially elongated along the diagonal line, but they acquire a squarelike shape at longer waiting times, such as T_w = 68.0 ps in Figure 2. The square shapes observed in the three samples evidence the growth of cross peaks in the 2DIR at a later waiting time, which are absent at T_w = 0 ps. These cross peaks are approximately located at (ω_τ, ω_t) = (2040, 2075 cm^{-1}) and (2080, 2055 cm^{-1}), which are circled in the spectra at 68 ps (Figure 2).

The 2DIR spectra of BSCN in different solvents are less complex than those of TBASCN. As a whole, the 2DIR spectra show a pair of positive and negative peaks with an elliptical shape, which are tilted and elongated along the diagonal line at early waiting times (Figure 3). At longer waiting times, the positive and negative peaks exhibit a change in their shape, since the peaks become fairly round after 68 ps. However, a close inspection of the peak shapes demonstrates that the peaks become rounder at different times for the different samples. For example, the peaks in the spectra of the NMA solution appear to be round at T_w = 68 ps, while the corresponding peaks for the DES2 and DES4 samples still exhibit slight elongations at this time. The change in the shape of the 2DIR peaks evidence the time evolution of spectral diffusion due to the dynamics in the solvation shell of BSCN. Notably, the 2DIR spectra of BSCN do not show any obvious signature of the presence of cross peaks within 100 ps waiting time.

The corresponding 2DIR spectra in the CO asymmetric stretching region of $W(CO)_6$ are shown in Figure 4. Consistent with FTIR spectra (Figure 1), the metal carbonyl shows a single band in this region as depicted by a single pair of positive and negative peaks. As in the case of BSCN, the positive and negative peaks are elongated along the diagonal line at shorter waiting times, but they become more upright and rounder at a longer waiting time. The 2DIR peak shapes do not present any clear evidence of cross peaks nor any obvious change after the waiting time of 69.7 ps. However, in the region of the side band (~2020 cm^{-1}), the growth of cross peaks between the side band and the main band of CO asymmetric stretch is observed (see the Supporting Information).

DISCUSSION

Ionic Solute (TBASCN). The structure of neat NMA−LA DES has been shown to be heterogeneous at the molecular level.[40] In particular, it has been shown that NMA and LA are likely to form polar and nonpolar domains, respectively. Thus, it is expected that thiocyanate and tetrabuthylammonium ions will reside in the polar domain of NMA−LA DES. The asymmetric peaks of the CN stretch in FTIR (Figure 1) and the cross peaks in the 2DIR spectra (Figure 2) at long waiting times indicate that thiocyanate ions have two underlying peaks within the CN stretch band, which are attributed to two different hydrogen bonded states of the ion. It has been previously shown that when the thiocyanate ion forms hydrogen bonds with solvent molecules, it exhibits two bands in the IR spectrum, corresponding to the ions with and without hydrogen bonds at high- and low-frequency sides,

https://dx.doi.org/10.1021/acs.jpcb.0c02482
J. Phys. Chem. B 2020, 124, 4762−4773

respectively.[43,47,73,74] The assignment of the peaks to thiocyanate ions with different number of hydrogen bonds is consistent with the presence of cross peaks at later waiting times due to the process of chemical exchange, in which some of the thiocyanate ions change their number of hydrogen bonds (vibrational state) during the waiting time. The switch of the hydrogen bond state and its corresponding vibrational frequencies give rise to the observed cross peaks.[64,75−77] While the formation of ionic aggregates can also result in more than one transition in the CN stretching region,[78] the low concentration of the solute (i.e., ∼100 mM) and the high polarity of NMA make it unlikely that ionic aggregates are formed in these solutions. Moreover, the absence of the cross peaks at waiting time zero further supports a mechanism of chemical exchange instead of the vibrational coupling expected from the formation of aggregates.[64,79]

The IR spectra of TBASCN (Figure 1) shows an apparent broadening of the CN stretch with decreasing concentration of NMA. A broadening in an IR line shape could indicate an increase in the heterogeneity and/or a slowdown in the dynamics around the anion. However, the presence of two bands in the CN stretching region does not allow us to directly identify the molecular origin of such broadening. For example, a larger splitting between these two bands can also result in a broader line shape. To discern between the two possible broadening mechanisms, the dynamics of the frequency−frequency correlation function (FFCF) was extracted by the photon echo peak shift.[64] It is important to note that the presence of overlapping transitions interferes with the analysis of the time evolution of spectral diffusion, and the use of peak shift provides average time constants for both thiocyanate CN stretches. The peak shift for different waiting times is shown in Figure 5a. The data was well-modeled with a double-exponential decay of the form:

$$y = A_1\, e^{-T_w/\tau_1} + A_2\, e^{-T_w/\tau_2} \quad (1)$$

where A_1 and A_2 are the amplitude, T_w is the waiting time, and τ_1 and τ_2 are the decorrelation times. The fitting parameters listed in Table 2 reveal a fast component (τ_1) in the dynamics of the thiocyanate stretch ascribed to the in-place motion or rotation of the ion and a slow component (τ_2) corresponding to the rearrangement of the solvent structure in the solvation shell of the anion.[73,80] In addition, it is apparent that the time constants (τ_1 or τ_2) do not differ significantly, while the amplitude (contribution) of each dynamical component does. In particular, an interplay between the two components is noticed as the decrease in the contribution from the slow dynamical component is followed by an increase in the contribution from the fast dynamical component when the concentration of NMA is increased. To evaluate the overall dynamics of the ionic solute, the weighted average of time constants, $\langle\tau_{avg}\rangle$, was calculated (Table 2). The weighted-average time constants show that the thiocyanate ion presents a slower dynamics when the concentration of NMA decreases, which is in line with the peak shift dynamics (Figure 5). Thus, the slowdown in dynamics with decreasing amount of NMA may explain the broadening of thiocyanate CN stretch observed in the linear spectra (Figure 1a).

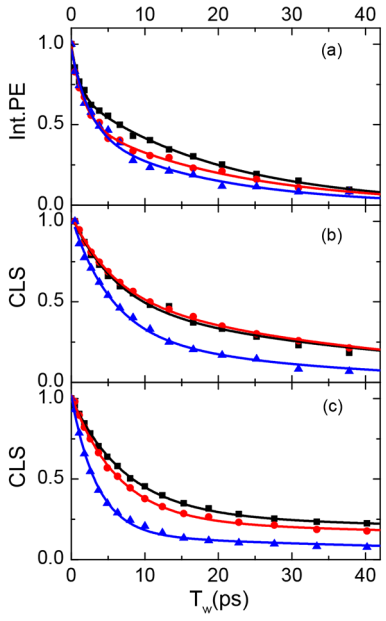

Figure 5. Metrics of the frequency−frequency correlation decay of three solutes in DES2 (black squares), DES4 (red circles), and NMA (blue triangles). (a) Photon echo peak shifts for nitrile stretch of TBASCN, (b) CLS of nitrile stretch in BSCN, and (c) CLS of carbonyl asymmetric stretch in $W(CO)_6$. Lines represent the models as described in the text. All data were normalized for comparison purposes.

The slowdown in the dynamics observed in NMA with the addition of LA to the system is in agreement with the confinement model previously proposed for NMA−LA DES[40] and is similar to that observed for reverse micelles.[81−83] However, in this case the polar domain forms the continuous phase (see Scheme 2), which is still confined due to the close proximity of the nonpolar domains as observed via small-angle X-ray scattering.[40] On the basis of the confinement model, an increase in the concentration of NMA results in larger continuous polar domain, which weakens the effect of the interface on the dynamics of this confined domain. As a result, the motion of the ionic solute inside the polar domain is less constrained, which results in faster dynamics.

Other dynamical information that can be retrieved from 2DIR spectra is the rate of growth of cross peaks. As discussed before, the cross peaks arise from the chemical exchange of thiocyanate ions with different number of hydrogen bonds. The cross peak growth as a function of the waiting time (Figure 6) shows its expected exponential growth, which is well-modeled with a function of the form:

$$y = A\,(1 - e^{-T_w/\tau_{cp}}) \quad (2)$$

where A is the amplitude, T_w is the waiting time, and τ_{cp} is the characteristic time of cross peak growth. The results of the modeling with eq 2 show that the time constants for hydrogen bond making and breaking in the two DESs and NMA are statistically the same (Table 2). This result is surprising given that there is a clear change in the solvation dynamics with NMA concentration. Interestingly, there has been a previous study on the confinement effect that showed a significant slowdown of water hydrogen bond making and breaking in confined systems.[81−84] However, it is also possible that the close proximity between the two transitions undergoing chemical exchange and spectral diffusion simultaneously makes the retrieval of dynamics constant less accurate. Nevertheless, the experimental data show that the chemical

https://dx.doi.org/10.1021/acs.jpcb.0c02482
J. Phys. Chem. B 2020, 124, 4762−4773

Table 2. Fitting Parameters of the FFCF and Chemical Exchange Processes Observed by TBASCN in the Different Environments

	FFCF					chemical exchange
sample	A_1	τ_1 (ps)	A_2	τ_2 (ps)	$\langle\tau_{avg}\rangle$ (ps)	τ_{cp} (ps)
DES2	0.30 ± 0.01	1.1 ± 0.1	0.70 ± 0.01	20 ± 1	14.3 ± 0.6	4.6 ± 0.3
DES4	0.45 ± 0.03	1.7 ± 0.2	0.53 ± 0.02	20 ± 1	11.6 ± 0.5	4.5 ± 0.3
NMA	0.50 ± 0.06	2.5 ± 0.5	0.47 ± 0.07	18 ± 3	10.0 ± 1.8	5.3 ± 0.7

Scheme 2. Cartoon Representation of Domains of the DES and Their Shared Interface[a]

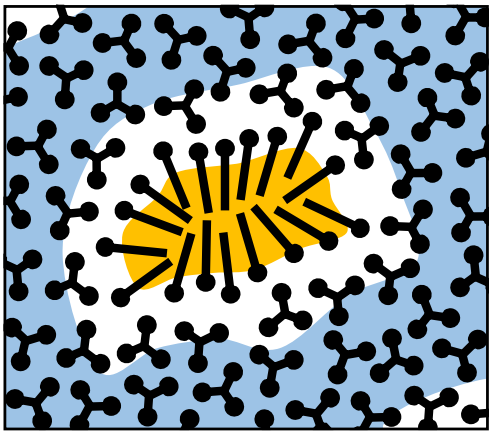

[a]Polar (blue) and non-polar (yellow) domains of the DES and their shared interface (green stripes); drum sticks and "Y" symbols represent the LA and NMA molecules, respectively.

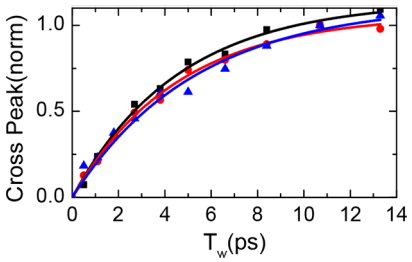

Figure 6. Cross peak growth with waiting time in 2DIR of TBASCN in DES2 (black squares), DES4 (red circles), and NMA (blue triangles). Lines represent the models of cross peak growth as described in text.

exchange rates of hydrogen bond making and breaking have characteristic times of a few picoseconds. These exchange rates are in agreement with the fast decay of the FFCF caused by tumbling (rotation) of the ion, since it is likely that the free rotation of the ion occurs simultaneously with the making and breaking of the hydrogen bonds between the thiocyanate ion and the amide. Overall, the observed relations between the dynamics and the concentration of NMA in the different DESs, as well as the presence of cross peaks due to chemical exchange between different hydrogen bond species, support our assignment of TBASCN solute residing in the polar (NMA) domain (see Scheme 2).

Molecular Polar Solute (BSCN). Generally, molecules containing nitrile groups show a solvatochromic shift in central frequency of the CN stretch due to the vibrational Stark effect.[85] While this is also true for the BSCN sample, the frequency maximum of the CN stretch changes slightly with solvent (see the Supporting Information), which is in agreement with the IR observations in a similar molecule.[55] This indicates that the CN stretch of BSCN is not a very sensitive solvatochromic probe, but it should still reveal the type of local environment via the position of the central frequency of this mode. The FTIR spectra of BSCN in the CN stretching frequency region for the DESs and neat NMA solutions (Figure 1b) show that the CN stretch central frequency (~2155−2156 cm^{-1}) is similar to that of ethyl acetate (~2156 cm^{-1}; see the Supporting Information), indicating that BSCN is in an environment analogous to that of a neat ester solution.

The small sensitivity of the CN stretch of BSCN to the environment via its frequency location allows us to infer some properties of its location from FTIR spectra, such as the mean local electric field.[86] In addition, the fwhm of the CN stretch of BSCN in the DESs and neat NMA is lower than that observed for methanol but higher than that for ethyl acetate (see the Supporting Information). While it is likely that BSCN does not form hydrogen bonds as seen from its fwhm, the linear IR is not sufficient to properly assess the presence of this interaction. To this end, the interactions between the CN group of BSCN and the environment in neat NMA and DESs were derived from the 2DIR spectra (Figure 3). Interestingly, the 2DIR spectra show only one transition with no apparent cross peaks. The dynamics of the spectral diffusion (Figure 5) derived from the center line slope (CLS)[87] reveals that the system has picosecond dynamics with more than one dynamical component. Moreover, it is easily observed from the CLS that BSCN has very similar dynamics in DES2 and DES4 (Figure 5), which significantly differs from that of the NMA solution. Modeling of the waiting time evolution of the CLS with a double-exponential decay (eq 1) reveals that the amplitudes and time constants of the correlation decay (Table 3) in DES2 and DES4 are statistically identical but different from those obtained for the solute in NMA.

Table 3. Fitting Parameters of Double-Exponential Decay for the CLS of BSCN in 2DIR Spectra

	FFCF			
sample	A_1	τ_1 (ps)	A_2	τ_2 (ps)
DES2	0.55 ± 0.06	6.0 ± 1.0	0.48 ± 0.06	47 ± 7
DES4	0.50 ± 0.03	5.7 ± 0.5	0.54 ± 0.03	43 ± 3
NMA	0.72 ± 0.07	5.3 ± 0.7	0.31 ± 0.08	29 ± 7

It is apparent that the polar solute (BSCN) not only senses the local environment but also provides information on the dynamics of the environment as previously demonstrated for methyl thiocyanate.[55] Thus, the similarity of the central frequency to that of an ester group and the statistically identical dynamics of the CN vibrational stretch in the two DESs with different compositions can be explained by locating the solute within the interface between the polar and nonpolar domains. In this case, it is expected that the ratio of two

https://dx.doi.org/10.1021/acs.jpcb.0c02482
J. Phys. Chem. B 2020, 124, 4762−4773

components will not influence the dynamics because the dynamics is determined by the interface itself rather than by the DES composition.[88,89] From a molecular point of view, the location of the BSCN solute in the interface is logical, since it is likely that in this location the benzyl ring of BSCN will align along the direction of carbon chains in the nonpolar domain, while its SCN group will be pointing toward the polar domain. Moreover, it is likely that in the interface the polar solute will not form hydrogen bonds with the LA carboxylic acid groups because the acid groups will be directly interacting with NMA as previously demonstrated in the neat DES.[40] This molecular picture is also in agreement with the lack of cross peaks in the 2DIR spectra of BSCN (Figure 3). In comparison to the ionic solute TBASCN, BSCN has a significantly different solvation structure in DES. Similar results were also found for organic and inorganic solutes in ionic liquids, where it was reported that organic and inorganic azides have very different solvation structures in a series of homologous imidazolium ionic liquids.[90]

Nonionic and Nonpolar Solute ($W(CO)_6$). The last solute investigated is the nonpolar molecular solute $W(CO)_6$. Previous studies have demonstrated that $W(CO)_6$ is a nonpolar solute having a high affinity to hydrophobic domains.[49−53] In particular, those studies relied on the degenerate CO asymmetric vibrational stretch in $W(CO)_6$ located at ∼1982 cm^{-1}. The FTIR of $W(CO)_6$ also shows a band in the same region but located at ∼1978 cm^{-1}, which is ∼4 cm^{-1} lower than the frequency in the hydrophobic domains. In addition, the CO asymmetric stretch band has a fwhm of ∼20 cm^{-1} in both DESs and neat NMA, which is twice the width reported for the same solute in a hydrophobic environment formed by lipid bilayers or oil phase of microemulsions.[49−53] The last finding is surprising considering that $W(CO)_6$ is a nonpolar solute and has always been observed within the hydrophobic domain.[49−53]

The effect of the local environment on $W(CO)_6$ was further investigated by dissolving the solute in hexane, ethyl acetate, and their mixtures to mimic the nonpolar and polar domains in DESs (see the Supporting Information). The CO asymmetric stretching region in these solvents reveals that the band shows not only a redshift in the central frequency but also a broadening with an increase in the concentration of ethyl acetate. In addition, the change in solvent from neat hexane to neat acetate exposes the growth of the high-frequency band at ∼2020 cm^{-1}, which matches the position of the side band as observed in the spectra of $W(CO)_6$ in the DESs and neat NMA. Interestingly, the bandwidth of the CO stretching in the DESs is closer to that of ethyl acetate than to hexane, indicating that $W(CO)_6$ is likely to reside close to the carboxylic or amide groups and away from the alkyl tails of LA.

A comparison of the fwhm of the CO asymmetric stretching band in DES and neat NMA shows a broadening by ∼4 cm^{-1} from DES2 to neat NMA. The change in the bandwidth evidences that the solute experiences a local environment which either is more disordered or has slower dynamics. To evaluate these two possibilities, the dynamics of the molecular environment was derived from the 2DIR spectra. In this case, the dynamics of the FFCF of the CO asymmetric stretch was extracted using CLS method. This metrics shows clearly that the dynamics of the $W(CO)_6$ environment become significantly faster with increasing concentration of NMA in the solution. Modeling of the data with eq 1 reveals the presence of a two-dynamical process (Table 4). The fast dynamical component has a characteristic time on the order of a few picoseconds, but the second dynamical component is very slow with the characteristic times of few hundred picoseconds. Moreover, the slow components are significantly slower than those observed for the other two solutes, TBASCN and BSCN. In two-component solvation dynamics, the faster component is generally attributed to the fluctuations due to in-place motion.[91,92] It was mentioned earlier that the CO stretch of $W(CO)_6$ is a triply degenerate (T_{1u}) coupled mode.[57,58] The intramolecular energy transfer in $W(CO)_6$ between the degenerate modes of the CO stretch in heptane was reported to be ∼8 ps, while its anisotropy dynamics was 4.7 ps.[93] Similarly, in a polarization-dependent 2DIR study of guanidinium chloride in D_2O, a faster energy transfer between two nearly degenerate stretching mode of guanidinium cation was reported to happen in ∼0.5 ps.[94] Note that the energy transfer between the degenerate stretching modes of guanidinium cation was enabled by the breaking of symmetry in the environment. Therefore, the fast component observed in this study could have a contribution from the reorientation dynamics and the intramolecular energy transfer among the degenerate coupled IR modes of CO stretch.

Table 4. Fitting Parameters of Double-Exponential Decay for the CLS of $W(CO)_6$ in 2DIR Spectra

	FFCF			
sample	A_1	τ_1 (ps)	A_2	τ_2 (ps)
DES2	0.74 ± 0.01	7.6 ± 0.2	0.26 ± 0.01	226 ± 27
DES4	0.79 ± 0.01	6.3 ± 0.2	0.23 ± 0.01	175 ± 28
NMA	0.86 ± 0.02	3.5 ± 0.2	0.15 ± 0.01	72 ± 14

The slow motion of the molecular environment sensed by $W(CO)_6$ becomes faster with the addition of NMA. Moreover, there is a linear relation between the concentration of NMA in the solution and the characteristic times of the slow dynamical component (see the Supporting Information). The linear relation between the dynamics of the environment and NMA concentration could indicate that the probe resides either in the interface or in the polar domain formed by NMA. An increase in NMA concentration results in a faster dynamics of the environment, indicating that the probe is probably confined in the NMA (polar) domain. However, the confinement model used to describe the local environment of TBASCN will only be reasonable if the polar domain presents a molecular environment suitable for the $W(CO)_6$ to reside. Previously, it has been demonstrated that NMA forms clusters in the presence of water, where the methyl groups of the NMA molecules aggregate giving rise to a hydrophobic collapse.[95] Thus, it is possible that the NMA molecules arrange the methyl groups around the solute to form a hydrophobic pocket within the polar domain. The similarity between the bandwidth and central frequencies of the CO asymmetric stretch in the two DESs and neat NMA supports this idea. Moreover, the linear relation of the slow dynamics of the environment to the concentration of NMA can be explained within this context because the addition of LA creates more confined polar domains,[40] which have slower motions due to the larger effect of the interface.[81,96]

The broadening of the CO asymmetric stretch band seen in the IR spectra provides more evidence to the location of the nonpolar solute. The IR line shape broadening can be caused by changes in the vibrational dynamics. In particular, the CO asymmetric stretch of $W(CO)_6$ has a long vibrational lifetime,

https://dx.doi.org/10.1021/acs.jpcb.0c02482
J. Phys. Chem. B 2020, 124, 4762−4773

which results in a small contribution to the line shape width.[49] Thus, large variations in the FFCF dynamical components are expected to cause the observed line shape broadening for the CO asymmetric stretch of $W(CO)_6$. According to the Kubo line shape theory, the changes in the line shape could arise from variations in either the dynamics characteristic times, where slower dynamics results in broader bands or the frequency fluctuation amplitudes where large amplitudes also produce broader bands. In this case, the change in the dynamical characteristic times does not justify the observed broadening, since the largest bandwidth is observed for the solute in neat NMA, but the solute has the fastest dynamics in this solvent. Thus, only a more disordered structure in NMA as compared to the DES can explain the broadening of the band. The largest heterogeneity in the molecular environment sensed by $W(CO)_6$ may be due to the NMA (polar) domain restructuring induced by the addition of nonpolar solute. The idea of domain restructuring has been previously used to describe the effect of molecular probes in ionic liquids, where it was observed that a large probe, compared to solvent, may induce significant domain restructuring of the solvent.[97] While it is possible that the solute is residing at the interface, the changes in dynamics for the nonpolar solute in the DESs suggest that this is not the case. However, it is also possible that the domain restructuring involves a rearrangement of the interface. Thus, the current data does not provide a clear indication of the solute location, so a more detailed study is needed to properly assess the location and effect of the nonpolar solute on the DES.

Another interesting feature observed in the FTIR of $W(CO)_6$ in DESs and neat NMA is the presence of a side band at ~2020 cm^{-1} as shown in Figure 1. This side band has cross peaks with the CO asymmetric stretching mode in 2DIR spectra (see the Supporting Information), which grows with a characteristic time of ~0.6 ps. While the side band could arise from the formation of $W(CO)_6$ dimers or aggregates, a dilution experiment in DES4 reveals that the side band remains after a 100-fold dilution, eliminating the possibility of dimer/aggregate formation. Another possibility is that the side band arises from the symmetric stretch transitions, which become weakly allowed due to a distortion in the symmetry of the $W(CO)_6$ molecule. In this case, the distortion in the molecular symmetry of the solute is not due to changes in its molecular geometry but due to the asymmetry in the environment. To support this hypothesis, DFT computations on a single $W(CO)_6$ molecule with one NMA were carried out. The results (see the Supporting Information) show that the nonallowed symmetric CO stretches become weakly allowed in the presence of an asymmetric environment. Moreover, the frequency separation between the asymmetric and symmetric stretching modes is ~40 cm^{-1} from DFT computation, which agrees very well with the frequency separation observed in IR experiments (Figure 1). The calculation also predicts a ratio of transition dipole moment intensities between the symmetric and asymmetric stretches of 0.06, which is comparable with the 0.04 deduced from the experiments (not shown). Hence, the side band is assigned to the two symmetric CO stretches of $W(CO)_6$, which is due to an asymmetry in the solvation shell becoming weakly allowed and having cross peaks with the asymmetric CO stretches of $W(CO)_6$ via either vibrational energy transfer between symmetric and asymmetric modes[98−101] and/or a mechanism involving low-frequency vibrational modes.[102] Interestingly, the symmetric CO stretch (Raman active) was previously reported to be ~42 cm^{-1} higher than the asymmetric CO stretch (IR active).[59] In an asymmetric environment, the symmetry of the environment could "turn on" the IR activity of the symmetric stretch mode as it is revealed in our result. Moreover, the vibrational energy transfer between these asymmetric and symmetric CO stretches was observed previously for $W(CO)_6$ in *n*-hexane.[57] The most interesting aspect of the presence of the symmetric CO stretches of $W(CO)_6$ is the requirement of an asymmetric solvation shell around the solute, indicating that in both DESs and NMA the nonpolar solute is sensing a very heterogeneous molecular environment.

SUMMARY

The nanoscopic molecular structure of nonionic NMA−LA DES was probed using three different solutes with varying polarities. In this study, three probes in the DESs with different compositions were investigated by linear and time-resolved infrared spectroscopies in order to study the change in structure and dynamics of DESs with varying mixing ratio. It is shown that solutes with different polarities are located in different domains of DES. In particular, it is found that the ionic solute (TBASCN) resides in the polar continuous domain formed by NMA and experiences a confinement effect when the concentration of NMA changes. In the case of the polar nonionic solute (BSCN), the result indicates that the solute is likely to reside in the interface. Finally, the results from the nonionic solute ($W(CO)_6$), contrary to previous reports, do not indicate that it positions itself within the LA nonpolar domain. The experimental results point to the probe inducing a domain restructuring, which results in a hydrophobic domain within the NMA continuous domain through hydrophobic collapse. This molecular picture is in agreement with the confinement effect observed in its dynamics. However, to confirm the proposed location, further investigation on this solute in the NMA−LA DES via molecular dynamics simulation is planned for the future.

ASSOCIATED CONTENT

Supporting Information

The Supporting Information is available free of charge at https://pubs.acs.org/doi/10.1021/acs.jpcb.0c02482.

FTIR parameters of three solutes in DESs and NMA (Table S1), FTIR parameters of BSCN in various solvents (Table S2), fitting parameters of cross peak growth (Table S3), DFT frequency calculation of single $W(CO)_6$ (Table S4), DFT frequency calculation of $W(CO)_6$ with one NMA (Table S5), viscosity of DES2, DES4 and NMA (Table S6), FTIR parameters of $W(CO)_6$ in various solvents (Table S6), second derivative of TBASCN spectra (Figure S1), FTIR spectra of BSCN in different solvents (Figure S2), 2DIR cross peaks between symmetric and asymmetric CO stretch of $W(CO)_6$ (Figure S3), cross peak growth in 2DIR spectra of $W(CO)_6$ (Figure S4), FTIR spectra of $W(CO)_6$ in mixtures of hexane and ethyl acetate (Figure S5), relation between concentration of NMA and characteristic time constants of $W(CO)_6$ (Figure S6), FTIR of dilute solution of $W(CO)_6$ in DES4 (Figure S7), optimized structures of $W(CO)_6$ and $W(CO)_6$ with one NMA (Figure S8), and FTIR spectra of $W(CO)_6$ in different solvent (Figure S8) (PDF)

https://dx.doi.org/10.1021/acs.jpcb.0c02482
J. Phys. Chem. B 2020, 124, 4762−4773

AUTHOR INFORMATION

Corresponding Author

Daniel G. Kuroda − *Department of Chemistry, Louisiana State University, Baton Rouge, Louisiana 70803, United States;* orcid.org/0000-0002-4752-7024; Phone: (+1) 225-578-1780; Email: dkuroda@lsu.edu

Authors

Xiaobing Chen − *Department of Chemistry, Louisiana State University, Baton Rouge, Louisiana 70803, United States*

Yaowen Cui − *Department of Chemistry, Louisiana State University, Baton Rouge, Louisiana 70803, United States*

Habtom B. Gobeze − *Department of Chemistry, Louisiana State University, Baton Rouge, Louisiana 70803, United States*

Complete contact information is available at: https://pubs.acs.org/10.1021/acs.jpcb.0c02482

Author Contributions

†X.C. and Y.C. contributed equally to this work.

Notes

The authors declare no competing financial interest.

ACKNOWLEDGMENTS

The current work was supported in part by the LSU Department of Chemistry and by the ACS - Petroleum Research Fund grant 56529-DNI6. The authors acknowledge financial support from the LSU Chemistry Department. The authors also acknowledge the High Performance Computing Center at Louisiana State University and the Louisiana Optical Network Initiative (LONI) for computer time.

REFERENCES

(1) Smith, E. L.; Abbott, A. P.; Ryder, K. S. Deep Eutectic Solvents (DESs) and Their Applications. *Chem. Rev.* **2014**, *114* (21), 11060−11082.

(2) Yan, Y. C.; W, R.; Khalid, M.; Shahbaz, K.; Gupta, T.; Mase, N. Potential application of deep eutectic solvents in heat transfer application. *Int. J. Eng. Sci. Technol.* **2017**, *12*, 1−14.

(3) Shahbaz, K.; Mjalli, F. S.; Hashim, M. A.; AlNashef, I. M. Prediction of deep eutectic solvents densities at different temperatures. *Thermochim. Acta* **2011**, *515* (1), 67−72.

(4) Marcus, Y. The Variety of Deep Eutectic Solvents. In *Deep Eutectic Solvents*; Springer International Publishing: Cham, 2019; pp 13−44.

(5) Tomé, L. I. N.; Baião, V.; da Silva, W.; Brett, C. M. A. Deep eutectic solvents for the production and application of new materials. *Appl. Mater. Today* **2018**, *10*, 30−50.

(6) Shishov, A.; Bulatov, A.; Locatelli, M.; Carradori, S.; Andruch, V. Application of deep eutectic solvents in analytical chemistry. A review. *Microchem. J.* **2017**, *135*, 33−38.

(7) Abbott, A. P.; Capper, G.; Davies, D. L.; Rasheed, R. K.; Tambyrajah, V. Novel solvent properties of choline chloride/urea mixtures. *Chem. Commun.* **2003**, *1*, 70−71.

(8) Cui, Y.; Li, C.; Yin, J.; Li, S.; Jia, Y.; Bao, M. Design, synthesis and properties of acidic deep eutectic solvents based on choline chloride. *J. Mol. Liq.* **2017**, *236*, 338−343.

(9) Kudłak, B.; Owczarek, K.; Namieśnik, J. Selected issues related to the toxicity of ionic liquids and deep eutectic solvents—a review. *Environ. Sci. Pollut. Res.* **2015**, *22* (16), 11975−11992.

(10) Khandelwal, S.; Tailor, Y.; Kumar, M. Deep Eutectic Solvents (DESs) as Eco-Friendly and Sustainable Solvent/Catalyst Systems in Organic Transformations. *J. Mol. Liq.* **2016**, *215*, 345−386.

(11) Durand, E.; Lecomte, J.; Villeneuve, P. Deep eutectic solvents: Synthesis, application, and focus on lipase-catalyzed reactions. *Eur. J. Lipid Sci. Technol.* **2013**, *115* (4), 379−385.

(12) Handy, S. T., Deep eutectic solvents in organic synthesis. In *Ionic Liquids−Current State of the Art*; Handy, S., Ed.; BoD − Books on Demand, 2015.

(13) Alonso, D. A.; Baeza, A.; Chinchilla, R.; Guillena, G.; Pastor, I. M.; Ramón, D. J. Deep eutectic solvents: the organic reaction medium of the century. *Eur. J. Org. Chem.* **2016**, *2016* (4), 612−632.

(14) Liu, P.; Hao, J.-W.; Mo, L.-P.; Zhang, Z.-H. Recent advances in the application of deep eutectic solvents as sustainable media as well as catalysts in organic reactions. *RSC Adv.* **2015**, *5* (60), 48675−48704.

(15) Handy, S.; Lavender, K. Organic synthesis in deep eutectic solvents: Paal−Knorr reactions. *Tetrahedron Lett.* **2013**, *54* (33), 4377−4379.

(16) Massolo, E.; Palmieri, S.; Benaglia, M.; Capriati, V.; Perna, F. M. Stereoselective organocatalysed reactions in deep eutectic solvents: highly tunable and biorenewable reaction media for sustainable organic synthesis. *Green Chem.* **2016**, *18* (3), 792−797.

(17) del Monte, F.; Carriazo, D.; Serrano, M. C.; Gutiérrez, M. C.; Ferrer, M. L. Deep Eutectic Solvents in Polymerizations: A Greener Alternative to Conventional Syntheses. *ChemSusChem* **2014**, *7* (4), 999−1009.

(18) Abo-Hamad, A.; Hayyan, M.; AlSaadi, M. A.; Hashim, M. A. Potential applications of deep eutectic solvents in nanotechnology. *Chem. Eng. J.* **2015**, *273*, 551−567.

(19) Wagle, D. V.; Zhao, H.; Baker, G. A. Deep eutectic solvents: sustainable media for nanoscale and functional materials. *Acc. Chem. Res.* **2014**, *47* (8), 2299−2308.

(20) Carriazo, D.; Serrano, M. C.; Gutiérrez, M. C.; Ferrer, M. L.; del Monte, F. Deep-eutectic solvents playing multiple roles in the synthesis of polymers and related materials. *Chem. Soc. Rev.* **2012**, *41* (14), 4996−5014.

(21) Sharma, M.; Mukesh, C.; Mondal, D.; Prasad, K. Dissolution of α-chitin in deep eutectic solvents. *RSC Adv.* **2013**, *3* (39), 18149−18155.

(22) Francisco, M.; van den Bruinhorst, A.; Kroon, M. C. New natural and renewable low transition temperature mixtures (LTTMs): screening as solvents for lignocellulosic biomass processing. *Green Chem.* **2012**, *14* (8), 2153−2157.

(23) Xia, S.; Baker, G. A.; Li, H.; Ravula, S.; Zhao, H. Aqueous ionic liquids and deep eutectic solvents for cellulosic biomass pretreatment and saccharification. *RSC Adv.* **2014**, *4* (21), 10586−10596.

(24) Abbott, A. P.; Azam, M.; Ryder, K. S.; Saleem, S. In situ electrochemical digital holographic microscopy; a study of metal electrodeposition in deep eutectic solvents. *Anal. Chem.* **2013**, *85* (14), 6653−6660.

(25) Nkuku, C. A.; LeSuer, R. J. Electrochemistry in deep eutectic solvents. *J. Phys. Chem. B* **2007**, *111* (46), 13271−13277.

(26) Ballantyne, A. D.; Forrest, G. C. H.; Frisch, G.; Hartley, J. M.; Ryder, K. S. Electrochemistry and speciation of Au+ in a deep eutectic solvent: growth and morphology of galvanic immersion coatings. *Phys. Chem. Chem. Phys.* **2015**, *17* (45), 30540−30550.

(27) Lloyd, D.; Vainikka, T.; Kontturi, K. The development of an all copper hybrid redox flow battery using deep eutectic solvents. *Electrochim. Acta* **2013**, *100*, 18−23.

(28) Li, X.; Row, K. H. Development of deep eutectic solvents applied in extraction and separation. *J. Sep. Sci.* **2016**, *39* (18), 3505−3520.

(29) García, G.; Aparicio, S.; Ullah, R.; Atilhan, M. Deep eutectic solvents: physicochemical properties and gas separation applications. *Energy Fuels* **2015**, *29* (4), 2616−2644.

(30) Tang, B.; Zhang, H.; Row, K. H. Application of deep eutectic solvents in the extraction and separation of target compounds from various samples. *J. Sep. Sci.* **2015**, *38* (6), 1053−1064.

(31) Dai, Y.; Witkamp, G.-J.; Verpoorte, R.; Choi, Y. H. Natural deep eutectic solvents as a new extraction media for phenolic metabolites in Carthamus tinctorius L. *Anal. Chem.* **2013**, *85* (13), 6272−6278.

(32) Duan, L.; Dou, L.-L.; Guo, L.; Li, P.; Liu, E. H. Comprehensive Evaluation of Deep Eutectic Solvents in Extraction of Bioactive

Natural Products. *ACS Sustainable Chem. Eng.* **2016**, *4* (4), 2405−2411.
(33) Zhao, B.-Y.; Xu, P.; Yang, F.-X.; Wu, H.; Zong, M.-H.; Lou, W.-Y. Biocompatible Deep Eutectic Solvents Based on Choline Chloride: Characterization and Application to the Extraction of Rutin from Sophora japonica. *ACS Sustainable Chem. Eng.* **2015**, *3* (11), 2746−2755.
(34) Cai, T.; Qiu, H. Application of deep eutectic solvents in chromatography: A review. *TrAC, Trends Anal. Chem.* **2019**, *120*, 115623.
(35) Cui, Y. W.; Kuroda, D. G. Evidence of Molecular Heterogeneities in Amide-Based Deep Eutectic Solvents. *J. Phys. Chem. A* **2018**, *122* (5), 1185−1193.
(36) van Osch, D. J. G. P.; Zubeir, L. F.; van den Bruinhorst, A.; Rocha, M. A. A.; Kroon, M. C. Hydrophobic deep eutectic solvents as water-immiscible extractants. *Green Chem.* **2015**, *17* (9), 4518−4521.
(37) Cunha, S. C.; Fernandes, J. O. Extraction techniques with deep eutectic solvents. *TrAC, Trends Anal. Chem.* **2018**, *105*, 225−239.
(38) Ribeiro, B. D.; Florindo, C.; Iff, L. C.; Coelho, M. A. Z.; Marrucho, I. M. Menthol-based Eutectic Mixtures: Hydrophobic Low Viscosity Solvents. *ACS Sustainable Chem. Eng.* **2015**, *3* (10), 2469−2477.
(39) Cui, Y.; Li, M.-C.; Wu, Q.; Pojman, J. A.; Kuroda, D. G. Synthesis-Free Phase-Selective Gelator for Oil-Spill Remediation. *ACS Appl. Mater. Interfaces* **2017**, *9* (39), 33549−33553.
(40) Cui, Y.; Rushing, J. C.; Seifert, S.; Bedford, N. M.; Kuroda, D. G. Molecularly Heterogeneous Structure of a Nonionic Deep Eutectic Solvent Composed of N-Methylacetamide and Lauric Acid. *J. Phys. Chem. B* **2019**, *123* (18), 3984−3993.
(41) Das, A.; Das, S.; Biswas, R. Density relaxation and particle motion characteristics in a non-ionic deep eutectic solvent (acetamide + urea): Time-resolved fluorescence measurements and all-atom molecular dynamics simulations. *J. Chem. Phys.* **2015**, *142* (3), 034505.
(42) Ohta, K.; Tominaga, K. Vibrational population relaxation of thiocyanate ion in polar solvents studied by ultrafast infrared spectroscopy. *Chem. Phys. Lett.* **2006**, *429* (1), 136−140.
(43) Ren, Z.; Brinzer, T.; Dutta, S.; Garrett-Roe, S. Thiocyanate as a Local Probe of Ultrafast Structure and Dynamics in Imidazolium-Based Ionic Liquids: Water-Induced Heterogeneity and Cation-Induced Ion Pairing. *J. Phys. Chem. B* **2015**, *119* (13), 4699−4712.
(44) Lee, H.; Choi, J.-H.; Cho, M. Vibrational solvatochromism and electrochromism of cyanide, thiocyanate, and azide anions in water. *Phys. Chem. Chem. Phys.* **2010**, *12* (39), 12658−12669.
(45) Viswanath, P.; Motschmann, H. Effect of Interfacial Presence of Oriented Thiocyanate on Water Structure. *J. Phys. Chem. C* **2008**, *112* (6), 2099−2103.
(46) Viswanath, P.; Motschmann, H. Oriented Thiocyanate Anions at the Air−Electrolyte Interface and Its Implications on Interfacial Water - A Vibrational Sum Frequency Spectroscopy Study. *J. Phys. Chem. C* **2007**, *111* (12), 4484−4486.
(47) Wei, Q.; Zhou, D.; Li, X.; Chen, Y.; Bian, H. Structural Dynamics of Dimethyl Sulfoxide Aqueous Solutions Investigated by Ultrafast Infrared Spectroscopy: Using Thiocyanate Anion as a Local Vibrational Probe. *J. Phys. Chem. B* **2018**, *122* (50), 12131−12138.
(48) Touaj, K.; Chabanel, M. Aggregation of alkaline-earth-metal thiocyanates in aprotic donor solvents. *J. Chem. Soc., Faraday Trans.* **1995**, *91* (24), 4395−4401.
(49) Kel, O.; Tamimi, A.; Thielges, M. C.; Fayer, M. D. Ultrafast Structural Dynamics Inside Planar Phospholipid Multibilayer Model Cell Membranes Measured with 2D IR Spectroscopy. *J. Am. Chem. Soc.* **2013**, *135* (30), 11063−11074.
(50) Gironi, B.; Lapini, A.; Ragnoni, E.; Calvagna, C.; Paolantoni, M.; Morresi, A.; Sassi, P. Free volume and dynamics in a lipid bilayer. *Phys. Chem. Chem. Phys.* **2019**, *21* (41), 23169−23178.
(51) Kel, O.; Tamimi, A.; Fayer, M. D. Size-dependent ultrafast structural dynamics inside phospholipid vesicle bilayers measured with 2D IR vibrational echoes. *Proc. Natl. Acad. Sci. U. S. A.* **2014**, *111* (3), 918−923.
(52) Kel, O.; Tamimi, A.; Fayer, M. D. The Influence of Cholesterol on Fast Dynamics Inside of Vesicle and Planar Phospholipid Bilayers Measured with 2D IR Spectroscopy. *J. Phys. Chem. B* **2015**, *119* (29), 8852−8862.
(53) Zang, J.; Feng, M.; Zhao, J.; Wang, J. Micellar and bicontinuous microemulsion structures show different solute−solvent interactions: a case study using ultrafast nonlinear infrared spectroscopy. *Phys. Chem. Chem. Phys.* **2018**, *20* (30), 19938−19949.
(54) Galle Kankanamge, S. R.; Kuroda, D. G. Molecular structure and ultrafast dynamics of sodium thiocyanate ion pairs formed in glymes of different lengths. *Phys. Chem. Chem. Phys.* **2019**, *21* (2), 833−841.
(55) Maienschein-Cline, M. G.; Londergan, C. H. The CN Stretching Band of Aliphatic Thiocyanate is Sensitive to Solvent Dynamics and Specific Solvation. *J. Phys. Chem. A* **2007**, *111* (40), 10020−10025.
(56) Dalton, S. R.; Vienneau, A. R.; Burstein, S. R.; Xu, R. J.; Linse, S.; Londergan, C. H. Cyanylated Cysteine Reports Site-Specific Changes at Protein−Protein-Binding Interfaces Without Perturbation. *Biochemistry* **2018**, *57* (26), 3702−3712.
(57) Arrivo, S. M.; Dougherty, T. P.; Grubbs, W. T.; Heilweil, E. J. Ultrafast infrared spectroscopy of vibrational CO-stretch up-pumping and relaxation dynamics of W(CO)6. *Chem. Phys. Lett.* **1995**, *235* (3), 247−254.
(58) Tokmakoff, A.; Fayer, M. D. Infrared Photon Echo Experiments: Exploring Vibrational Dynamics in Liquids and Glasses. *Acc. Chem. Res.* **1995**, *28* (11), 437−445.
(59) Tokmakoff, A.; Sauter, B.; Kwok, A. S.; Fayer, M. D. Phonon-induced scattering between vibrations and multiphoton vibrational up-pumping in liquid solution. *Chem. Phys. Lett.* **1994**, *221* (5), 412−418.
(60) Tarif, E.; Mondal, J.; Biswas, R. Interaction and Dynamics in a Fully Biodegradable Glucose-Containing Naturally Abundant Deep Eutectic Solvent: Temperature-Dependent Time-Resolved Fluorescence Measurements. *J. Phys. Chem. B* **2019**, *123* (44), 9378−9387.
(61) Gautam, R. K.; Chatterjee, A.; Seth, D. Photophysics, rotational dynamics and fluorescence lifetime imaging study of coumarin dyes in deep eutectic solvent. *J. Mol. Liq.* **2019**, *280*, 399−409.
(62) Tarif, E.; Mondal, J.; Biswas, R. How frictional response during solute solvation controls solute rotation in naturally abundant deep eutectic solvent (NADES)? A case study with amino acid derivative containing DES. *J. Mol. Liq.* **2020**, *303*, 112451.
(63) Dhingra, D.; Bhawna; Pandey, A.; Pandey, S. Pyrene Fluorescence To Probe a Lithium Chloride-Added (Choline Chloride + Urea) Deep Eutectic Solvent. *J. Phys. Chem. B* **2019**, *123* (14), 3103−3111.
(64) Hamm, P.; Zanni, M. *Concepts and Methods of 2D Infrared Spectroscopy*; Cambridge University Press: Cambridge, 2011.
(65) Fayer, M. D. Dynamics of Liquids, Molecules, and Proteins Measured with Ultrafast 2D IR Vibrational Echo Chemical Exchange Spectroscopy. *Annu. Rev. Phys. Chem.* **2009**, *60* (1), 21−38.
(66) Asplund, M. C.; Zanni, M. T.; Hochstrasser, R. M. Two-dimensional infrared spectroscopy of peptides by phase-controlled femtosecond vibrational photon echoes. *Proc. Natl. Acad. Sci. U. S. A.* **2000**, *97* (15), 8219−8224.
(67) Eckbreth, A. C. BOXCARS: Crossed-beam phase-matched CARS generation in gases. *Appl. Phys. Lett.* **1978**, *32* (7), 421−423.
(68) Kim, Y. S.; Wang, J.; Hochstrasser, R. M. Two-Dimensional Infrared Spectroscopy of the Alanine Dipeptide in Aqueous Solution. *J. Phys. Chem. B* **2005**, *109* (15), 7511−7521.
(69) Frisch, M. J.; Trucks, G. W.; Schlegel, H. B.; Scuseria, G. E.; Robb, M. A.; Cheeseman, J. R.; Scalmani, G.; Barone, V.; Petersson, G. A.; Nakatsuji, H.; Li, X.; Caricato, M.; Marenich, A. V.; Bloino, J.; Janesko, B. G.; Gomperts, R.; Mennucci, B.; Hratchian, H. P.; Ortiz, J. V.; Izmaylov, A. F.; Sonnenberg, J. L.; Williams-Young, D.; Ding, F.; Lipparini, F.; Egidi, F.; Goings, J.; Peng, B.; Petrone, A.; Henderson, T.; Ranasinghe, D.; Zakrzewski, V. G.; Gao, J.; Rega, N.; Zheng, G.; Liang, W.; Hada, M.; Ehara, M.; Toyota, K.; Fukuda, R.; Hasegawa, J.; Ishida, M.; Nakajima, T.; Honda, Y.; Kitao, O.; Nakai, H.; Vreven, T.;

https://dx.doi.org/10.1021/acs.jpcb.0c02482
J. Phys. Chem. B 2020, 124, 4762−4773

Throssell, K.; Montgomery, J. A., Jr.; Peralta, J. E.; Ogliaro, F.; Bearpark, M.; Heyd, J. J.; Brothers, E. N.; Kudin, K. N.; Staroverov, V. N.; Kobayashi, R.; Normand, J.; Raghavachari, K.; Rendell, A.; Burant, J. C.; Iyengar, S. S.; Tomasi, J.; Cossi, M.; Millam, J. M.; Klene, M.; Adamo, C.; Cammi, R.; Ochterski, J. W.; Martin, R. L.; Morokuma, K.; Farkas, O.; Foresman, J. B.; Fox, D. J. *Gaussian 16*, revision C.01; Gaussian, Inc.: Wallingford CT, 2016.

(70) Ishikawa, Y.-i.; Kawakami, K. Structure and Infrared Spectroscopy of Group 6 Transition-Metal Carbonyls in the Gas Phase: DFT Studies on M(CO)n (M = Cr, Mo, and W; n = 6, 5, 4, and 3). *J. Phys. Chem. A* **2007**, *111* (39), 9940−9944.

(71) Banno, M.; Sato, S.; Iwata, K.; Hamaguchi, H.-o. Solvent-dependent intra- and intermolecular vibrational energy transfer of W(CO)6 probed with sub-picosecond time-resolved infrared spectroscopy. *Chem. Phys. Lett.* **2005**, *412* (4), 464−469.

(72) Jones, L. H.; McDowell, R. S.; Goldblatt, M. Force constants of the hexacarbonyls of chromium, molybdenum, and tungsten from the vibrational spectra of isotopic species. *Inorg. Chem.* **1969**, *8* (11), 2349−2363.

(73) Cui, Y.; Fulfer, K. D.; Ma, J.; Weldeghiorghis, T. K.; Kuroda, D. G. Solvation dynamics of an ionic probe in choline chloride-based deep eutectic solvents. *Phys. Chem. Chem. Phys.* **2016**, *18* (46), 31471−31479.

(74) Schultz, P. W.; Leroi, G. E.; Popov, A. I. Solvation of SCN- and SeCN- Anions in Hydrogen-Bonding Solvents. *J. Am. Chem. Soc.* **1996**, *118* (43), 10617−10625.

(75) Ji, M.; Odelius, M.; Gaffney, K. J. Large Angular Jump Mechanism Observed for Hydrogen Bond Exchange in Aqueous Perchlorate Solution. *Science* **2010**, *328* (5981), 1003−1005.

(76) Kim, Y. S.; Hochstrasser, R. M. Chemical exchange 2D IR of hydrogen-bond making and breaking. *Proc. Natl. Acad. Sci. U. S. A.* **2005**, *102* (32), 11185−11190.

(77) Kim, Y. S.; Hochstrasser, R. M. Applications of 2D IR Spectroscopy to Peptides, Proteins, and Hydrogen-Bond Dynamics. *J. Phys. Chem. B* **2009**, *113* (24), 8231−8251.

(78) Ji, M.; Park, S.; Gaffney, K. J. Dynamics of Ion Assembly in Solution: 2DIR Spectroscopy Study of LiNCS in Benzonitrile. *J. Phys. Chem. Lett.* **2010**, *1* (12), 1771−1775.

(79) Oudenhoven, T. A.; Joo, Y.; Laaser, J. E.; Gopalan, P.; Zanni, M. T. Dye aggregation identified by vibrational coupling using 2D IR spectroscopy. *J. Chem. Phys.* **2015**, *142* (21), 212449.

(80) Brinzer, T.; Garrett-Roe, S. Temperature and chain length dependence of ultrafast vibrational dynamics of thiocyanate in alkylimidazolium ionic liquids: A random walk on a rugged energy landscape. *J. Chem. Phys.* **2017**, *147* (19), 194501.

(81) Singh, P. K.; Kuroda, D. G.; Hochstrasser, R. M. An Ion's Perspective on the Molecular Motions of Nanoconfined Water: A Two-Dimensional Infrared Spectroscopy Study. *J. Phys. Chem. B* **2013**, *117* (33), 9775−9784.

(82) Tan, H.-S.; Piletic, I. R.; Riter, R. E.; Levinger, N. E.; Fayer, M. D. Dynamics of Water Confined on a Nanometer Length Scale in Reverse Micelles: Ultrafast Infrared Vibrational Echo Spectroscopy. *Phys. Rev. Lett.* **2005**, *94* (5), 057405.

(83) Moilanen, D. E.; Fenn, E. E.; Wong, D.; Fayer, M. D. Water Dynamics at the Interface in AOT Reverse Micelles. *J. Phys. Chem. B* **2009**, *113* (25), 8560−8568.

(84) Fayer, M. D.; Levinger, N. E. Analysis of Water in Confined Geometries and at Interfaces. *Annu. Rev. Anal. Chem.* **2010**, *3* (1), 89−107.

(85) Fried, S. D.; Boxer, S. G. Measuring Electric Fields and Noncovalent Interactions Using the Vibrational Stark Effect. *Acc. Chem. Res.* **2015**, *48* (4), 998−1006.

(86) Levinson, N. M.; Fried, S. D.; Boxer, S. G. Solvent-Induced Infrared Frequency Shifts in Aromatic Nitriles Are Quantitatively Described by the Vibrational Stark Effect. *J. Phys. Chem. B* **2012**, *116* (35), 10470−10476.

(87) Fenn, E. E.; Fayer, M. D. Extracting 2D IR frequency-frequency correlation functions from two component systems. *J. Chem. Phys.* **2011**, *135* (7), 074502.

(88) Fenn, E. E.; Wong, D. B.; Fayer, M. D. Water dynamics at neutral and ionic interfaces. *Proc. Natl. Acad. Sci. U. S. A.* **2009**, *106* (36), 15243−15248.

(89) Roy, V. P.; Kubarych, K. J. Interfacial Hydration Dynamics in Cationic Micelles Using 2D-IR and NMR. *J. Phys. Chem. B* **2017**, *121* (41), 9621−9630.

(90) Dutta, S.; Ren, Z.; Brinzer, T.; Garrett-Roe, S. Two-dimensional ultrafast vibrational spectroscopy of azides in ionic liquids reveals solute-specific solvation. *Phys. Chem. Chem. Phys.* **2015**, *17* (40), 26575−26579.

(91) Kwak, K.; Park, S.; Fayer, M. D. Dynamics around solutes and solute−solvent complexes in mixed solvents. *Proc. Natl. Acad. Sci. U. S. A.* **2007**, *104* (36), 14221−14226.

(92) Gupta, S.; Rafiq, S.; Sen, P. Dynamics of Solvent Response in Methanol−Chloroform Binary Solvent Mixture: A Case of Synergistic Solvation. *J. Phys. Chem. B* **2015**, *119* (7), 3135−3141.

(93) Banno, M.; Iwata, K.; Hamaguchi, H.-o. Intra- and intermolecular vibrational energy transfer in tungsten carbonyl complexes W(CO)5(X) (X═CO, CS, CH3CN, and CD3CN). *J. Chem. Phys.* **2007**, *126* (20), 204501.

(94) Vorobyev, D. Y.; Kuo, C.-H.; Kuroda, D. G.; Scott, J. N.; Vanderkooi, J. M.; Hochstrasser, R. M. Water-Induced Relaxation of a Degenerate Vibration of Guanidinium Using 2D IR Echo Spectroscopy. *J. Phys. Chem. B* **2010**, *114* (8), 2944−2953.

(95) Salamatova, E.; Cunha, A. V.; Bloem, R.; Roeters, S. J.; Woutersen, S.; Jansen, T. L. C.; Pshenichnikov, M. S. Hydrophobic Collapse in N-Methylacetamide−Water Mixtures. *J. Phys. Chem. A* **2018**, *122* (9), 2468−2478.

(96) Yuan, R. F.; Yan, C.; Nishida, J.; Fayer, M. D. Dynamics in a Water Interfacial Boundary Layer Investigated with IR Polarization-Selective Pump-Probe Experiments. *J. Phys. Chem. B* **2017**, *121* (17), 4530−4537.

(97) Jin, H.; Baker, G. A.; Arzhantsev, S.; Dong, J.; Maroncelli, M. Solvation and Rotational Dynamics of Coumarin 153 in Ionic Liquids: Comparisons to Conventional Solvents. *J. Phys. Chem. B* **2007**, *111* (25), 7291−7302.

(98) Chen, X.; Fulfer, K. D.; Woodard, K. T.; Kuroda, D. G. Structure and Dynamics of the Lithium-Ion Solvation Shell in Ureas. *J. Phys. Chem. B* **2019**, *123* (46), 9889−9898.

(99) Kuroda, D. G.; Abdo, M.; Chuntonov, L.; Smith, A. B., III; Hochstrasser, R. M. Vibrational dynamics of a non-degenerate ultrafast rotor: The (C12,C13)-oxalate ion. *J. Chem. Phys.* **2013**, *139* (16), 164514.

(100) Kuroda, D. G.; Hochstrasser, R. M. Two-dimensional infrared spectral signature and hydration of the oxalate dianion. *J. Chem. Phys.* **2011**, *135* (20), 204502.

(101) Fulfer, K. D.; Kuroda, D. G. A comparison of the solvation structure and dynamics of the lithium ion in linear organic carbonates with different alkyl chain lengths. *Phys. Chem. Chem. Phys.* **2017**, *19* (36), 25140−25150.

(102) Rubtsova, N. I.; Rubtsov, I. V. Vibrational Energy Transport in Molecules Studied by Relaxation-Assisted Two-Dimensional Infrared Spectroscopy. *Annu. Rev. Phys. Chem.* **2015**, *66*, 717−738.

https://dx.doi.org/10.1021/acs.jpcb.0c02482
J. Phys. Chem. B 2020, 124, 4762−4773